Journal of Radioanalytical and Nuclear Chemistry (2022) 331:2621–2629
https://doi.org/10.1007/s10967-022-08308-y

Transformation of radionuclide occurrence state in uranium and strontium recycling by *Saccharomyces cerevisiae*

Lei Zhou[1,2] · Faqin Dong[3] · Qunwei Dai[1] · Mingxue Liu[2] · Wei Zhang[3] · Yongde Zhang[1]

Received: 28 December 2021 / Accepted: 31 March 2022 / Published online: 21 May 2022

Abstract

Radionuclide recycling by biosorption combined with the ashing process is a promising nuclide recovery method. To investigate the transformation process of radionuclide occurrence state in bio-recycling, uranium and strontium recycling by *S.cerevisiae* were studied. *S. cerevisiae* exhibits good performance in the enrichment of uranium and strontium with as high as almost 90% biosorption efficiency. The results demonstrate that adsorbed uranium and strontium precipitates can be transformed into authenite and strontium sulfate on cell surface. The final state of uranium is mainly in form of UP_2O_7, while the final state of Sr(II) is mainly in form of $SrSO_4$ after ashing.

Graphic abstract

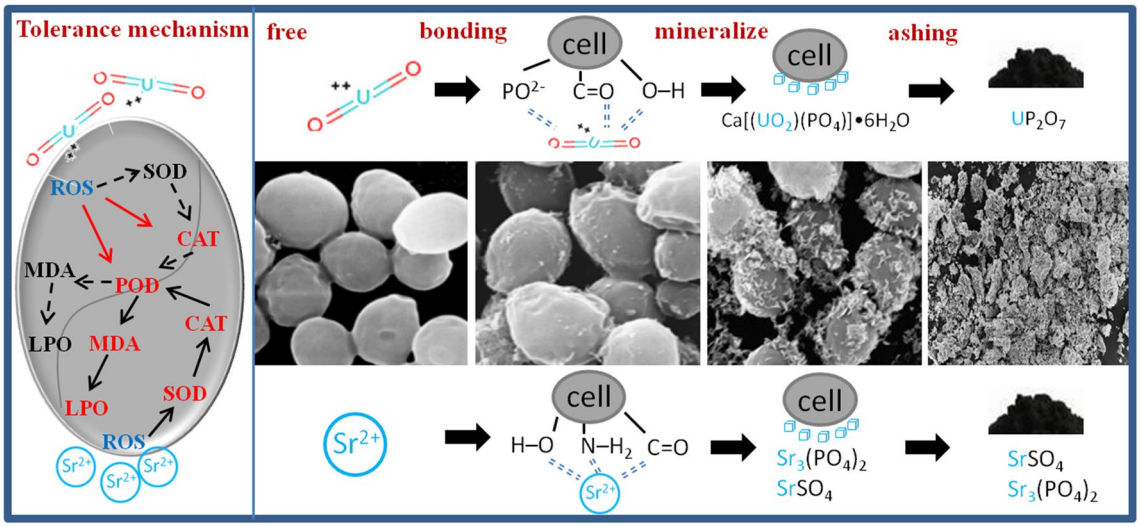

Keywords Uranium · Strontium · Bio-recycling · Occurrence state · Toxic effect

✉ Faqin Dong
fqdong@swust.edu.cn

[1] Fundamental Science on Nuclear Wastes and Environmental Safety Laboratory, Southwest University of Science and Technology, Mianyang 621010, Sichuan, China

[2] School of Life Science and Engineering, Southwest University of Science and Technology, 621010 Mianyang, Sichuan, China

[3] Key Laboratory of Solid Waste Treatment and the Resource Recycle, Southwest University of Science and Technology, Mianyang 621010, Sichuan, China

Introduction

The utilization and development of nuclear technology has brought great economic and social benefits to human beings but has also produced much more radioactive waste [1, 2]. Radionuclides could potentially harm the ecological environment and human health after they enter the water and soil environment [3, 4]. Biosorption is one of the most attractive and alternative methods for the removal of radioactive ions

and heavy metals from wastewater because it is not only cost effective but also provides an opportunity for the recycling of radionuclides [5, 6]. Compared with the traditional methods, biosorption is regarded as a promising and effective method for radionuclides remove, and *Saccharomyces cerevisiae* (*S. cerevisiae*) is one of the most promising biosorbent for its safety, low cost, high absorption capacity and easy obtain from fermentation industry [7]. In addition, the microorganism biosorption of radionuclide combined with the ashing process produced a great decrease in volume or weight and was more appropriate for use in solidification and geological disposal [8, 9].

Many researchers have studied the biosorption of heavy metals such as Cd, Cr, Cu, Mn, U, and Sr by *Saccharomyces cerevisiae* due to its outstanding biosorption performance [10–15]. Shen et al. found that uranium interacted with –O–H, –C=O and $–PO^{2-}$ on *Saccharomyces cerevisiae* surfaces, as well as culture medium, and formed uranium precipitates on cell surfaces [16]. The precipitate on the *Saccharomyces cerevisiae* surface was a uranium–phosphate compound in the form of a scale-like substance, and *Saccharomyces cerevisiae* could transform the uranium–phosphate precipitate into crystalline state-tetragonal chernikovite $[H_2(UO_2)_2(PO_4)_2{\cdot}8H_2O]$ [14]. Liu et al. found that the cell wall of *Saccharomyces cerevisiae* was the primary biosorption site where the adsorbed strontium ion was approximately 90% of the total adsorbed amount; the bioaccumulation in the cytoplasm varied by approximately 10% [15]. Hu et al. investigated the interaction between strontium and the mixed microorganisms of *Saccharomyces cerevisiae* and *Bacillus subtilis* and found that the hydroxyl, carboxyl, amino, and amide groups of microorganisms are the main active sites of the interface reactions [17]. The previous studies mainly aimed to improve biosorption capacity for heavy metals removal from industrial wastewater [18]. However, the transformation process of the radionuclide occurrence state from the water-soluble phase or ion phase, biosorption species, and precipitates to ashing products is not fully documented.

This study represents a comprehensive study in which uranium and strontium were recycled from the ion phase to the mineral phase by biosorption combined with the ashing process. The transformation of the radionuclide occurrence state in uranium and strontium recycling by *Saccharomyces cerevisiae* during the biosorption enrichment-separation-ashing process was investigated. The results of the study will help to design more efficient systems for bio-recycling uranium and strontium, which is not only cost effective but also have outstanding performance.

Materials and methods

Microorganism strain

The yeast *Saccharomyces cerevisiae* was provided by the Experiment Center of the Life Science and Engineering College, Southwest University of Science and Technology and domesticated in the laboratory under different uranium and strontium ion stresses.

Growth curves of *S. cerevisiae* and tolerance experiment solutions of uranium and strontium were mixed with suspensions of exponential phase *S. cerevisiae* and inoculated in Erlenmeyer flasks at 80 rpm and 30 ℃. The yeast culture medium was composed of 5% glucose, (0.1% $(NH_4)_2SO_4$, 0.1% urea, 0.05% yeast extract and 0.05% Na_2HPO_4 at pH 4.5. The initial uranium and strontium concentrations varied from 0 to 600 mg/L and were set at 0, 100, 200, 300, 400, and 500 mg/L by adding a certain quantity of uranyl acetate dihydrate $(UO_2(CH_3CO_2)_2{\cdot}2H_2O)$ and strontium nitrate $(Sr(NO_3)_2$ (AR, BeilianChem, China). Then, the cultures were placed in a constant temperature incubator. The OD values of culture samples were determined by a spectrophotometer at 560 nm wavelength every 2 h for 18 h. Each batch of domesticated experiments was performed in triplicate and contained blank controls.

Biosorption of uranium and strontium ions by *S. cerevisiae*

The biosorption experiment was performed according to our previous studies [5, 6, 8, 15]. In brief, *S. cerevisiae* culture, uranium and strontium addition methods were as described above ("Microorganism strain" section), and the pH was allowed to drift freely. After 24 h, the cell suspensions were centrifuged at 4000 rpm for 15 min (Eppendorf, Centrifuge 5804 R), and the residual uranium and strontium ion concentrations were measured by a spectrophotometer at 652 nm using arsenazoIII [19] and anatomic absorption spectrophotometer (PE AA700, Shelton, CT, USA). The sediments were washed twice with doubly distilled deionized water. Then, the sediments were dried using a vacuum freeze drier (cf. Labonco, USA) for 48 h.

The dried sample was analysed by scanning electron microscopy (SEM) coupled with EDX analysis according to Liu et al. (2010) and Fourier transform infrared spectroscopy (FTIR, Frontier). FTIR was conducted on dried samples of *S. cerevisiae* before and after biosorption and recorded on KBr pellets at room temperature using an FTIR spectrometer. Spectra ranging from 400 to 4000 cm^{-1} were obtained by coaddition of 64 scans with a resolution of 1 cm^{-1} and a mirror velocity of 0.6329 cm/s.

Ashing process

The collected *S. cerevisiae* cell sediments were rinsed with doubly distilled deionized water and then dried using hot air (40 ± 0.5 ℃). The dried sediment was carbonized in a crucible in an electrothermal furnace before ashing. The crucible containing *S. cerevisiae* cell sediments was placed in an electrothermal furnace (covered with an asbestos network) to heat the sediments. The heating process was completed until no smoke spread out, and then the crucible was placed on brick for cooling to room temperature. The carbonized sediment was placed into a muffle furnace (SX-4-10, Beijing Guangming Medical Instrument Co., Ltd., China) at 550–600 ℃ until all of the carbon had been oxidized and the weight was constant.

X-ray diffraction patterns of ashes were obtained by a PANalytical X'Pert PRO X-ray diffractometer (radius: 240.0 mm). Incident X-ray radiation was produced from a line-focused PW3373/10 Cu X-ray tube operating at 40 kV and 40 mA with Cu Kα radiation of 1.54 Å. The scan step size and time per step were 0.03° and 10.16 s, respectively.

Results and discussion

Enrichment of uranium and strontium by *S. cerevisiae*

The biosorption rate and biosorption capacity of *S. cerevisiae* to uranium and strontium at different initial concentrations were discussed (Fig. 1). The pH value has a vital role during uranium and strontium biosorption by *S. cerevisiae*, because the biosorption ability and the structure of uranium precipitation change significantly under different pH conditions [20, 21]. The zeta potential of *S. cerevisiae* was about − 25 mV at pH 4.5. The biosorption rate of *S. cerevisiae* to U(VI) was not linear with the initial uranium concentrations. The biosorption rate of *S. cerevisiae* to U(VI) was increased when uranium was at a low initial concentration. The biosorption rate of *S. cerevisiae* to U(VI) was the highest, up to 60%, when C_0 reached 10 mg/L. The biosorption rate of *S. cerevisiae* to U(VI) showed a nonlinear declining trend with increasing initial uranium concentration after it reached the maximum. The biosorption capacities of *S. cerevisiae* to U(VI) increased with increasing initial uranium concentration. The biosorption capacity per unit of *S. cerevisiae* to U(VI) was 320 mgU/g (D. W) when C_0 was 200 mg/L. Zhang et al. found that uranium biosorption of the protonated and chemically modified biomass of *S. cereisiae* also reached to nearly 100% biosorption rate at pH 4 [7].

In general, there were abundant biosorption points on the *S. cerevisiae* surface, and UO_2^{2+} could be easily absorbed when the UO_2^{2+} concentration was low. However, the biosorption efficiency of *S. cerevisiae* on U(VI) was unsatisfactory in a low concentration of uranium solution. This result showed that living microorganisms had a certain anti-biosorption capacity for low concentrations of uranium [14]. As the concentration of U(VI) increased, the toxicity of UO_2^{2+} to living microorganisms increased. Therefore, the biosorption resistance of living microorganism surfaces was broken, the number of active sites was changed, and a large amount of UO_2^{2+} was adsorbed. At the same time, the increase in uranium concentration provided a driving force for the barrier between the solid phase and liquid phase, and the effective biosorption points occupied by UO_2^{2+} on the surface of *S. cerevisiae* were promoted in the dynamic balance. Thus, the biosorption capacity of the bacterial cells was increased, and the limited active biosorption points tended to saturate while the biosorption rate was decreased.

As Fig. 1 left shows, the biosorption rate of strontium was strongly affected by the initial strontium concentration. A very different from U biosorption was that the

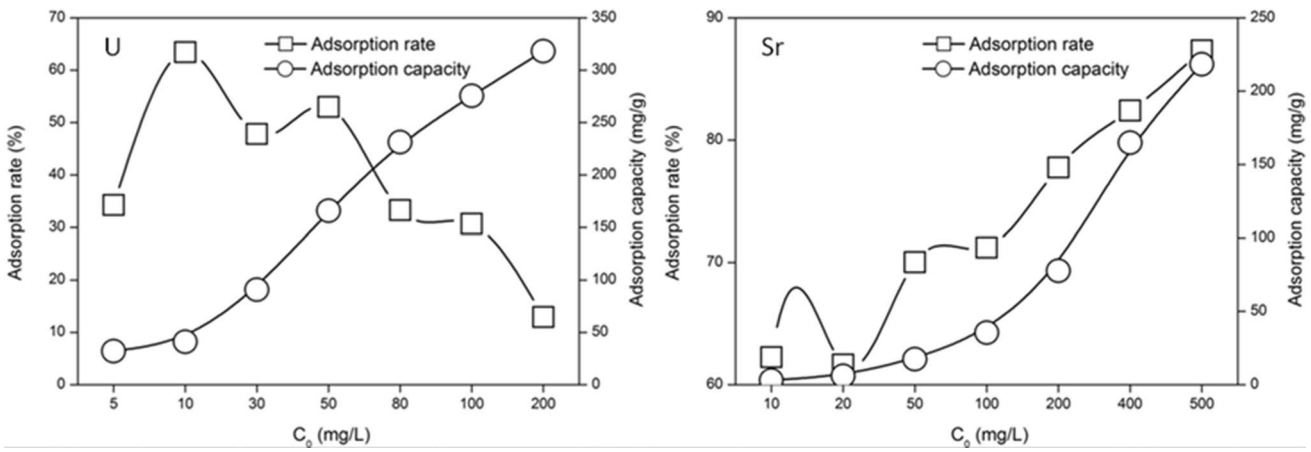

Fig. 1 Biosorption rate and biosorption capacity of *S. cerevisiae* with different initial uranium (right) and strontium (left) concentrations

biosorption rate always increased with initial strontium concentration from 10 to 500 mg/L. Qiu et al. examined the biosorption capacity of the K-0, K-4000, and Y-7 strains and found the maximum biosorption capacity of K-0 (12.227 mg g^{-1}) and K-4000 (12.172 mg g^{-1}) while the maximum biosorption capacity of K-0 was similar to K-4000 [13]. Also, it can be observed that the optimal culture time was 28–30 h for strontium (200 mg L^{-1}) under culture conditions. In addition to biosorption by *S. cerevisiae*, it might be caused by the strontium ion reaction with the culture medium components, for example, SO_4^{2-}, which could form the microsolubility salt $SrSO_4$ [22, 23].

Morphology characterization of uranium and strontium on *S. cerevisiae*

The SEM results (Fig. 2b) showed that the *S. cerevisiae* cell surface was covered with uranium precipitate compared with pristine cells (Fig. 2a). Merroun et al. observed that uranium precipitated while uranium was absorbed by *Bacillus sphaericus*, and the uranium precipitate was also located on the cell surface, similar to this study [24]. Uranium precipitate of outer membrane-peptidoglycan-plasma membrane complex as fine-grained, platy uranium minerals formed by Pseudomonas fluorescens was spread around entire Pseudomonas fluorescens cell [25]. As shown in Fig. 2b, the morphology

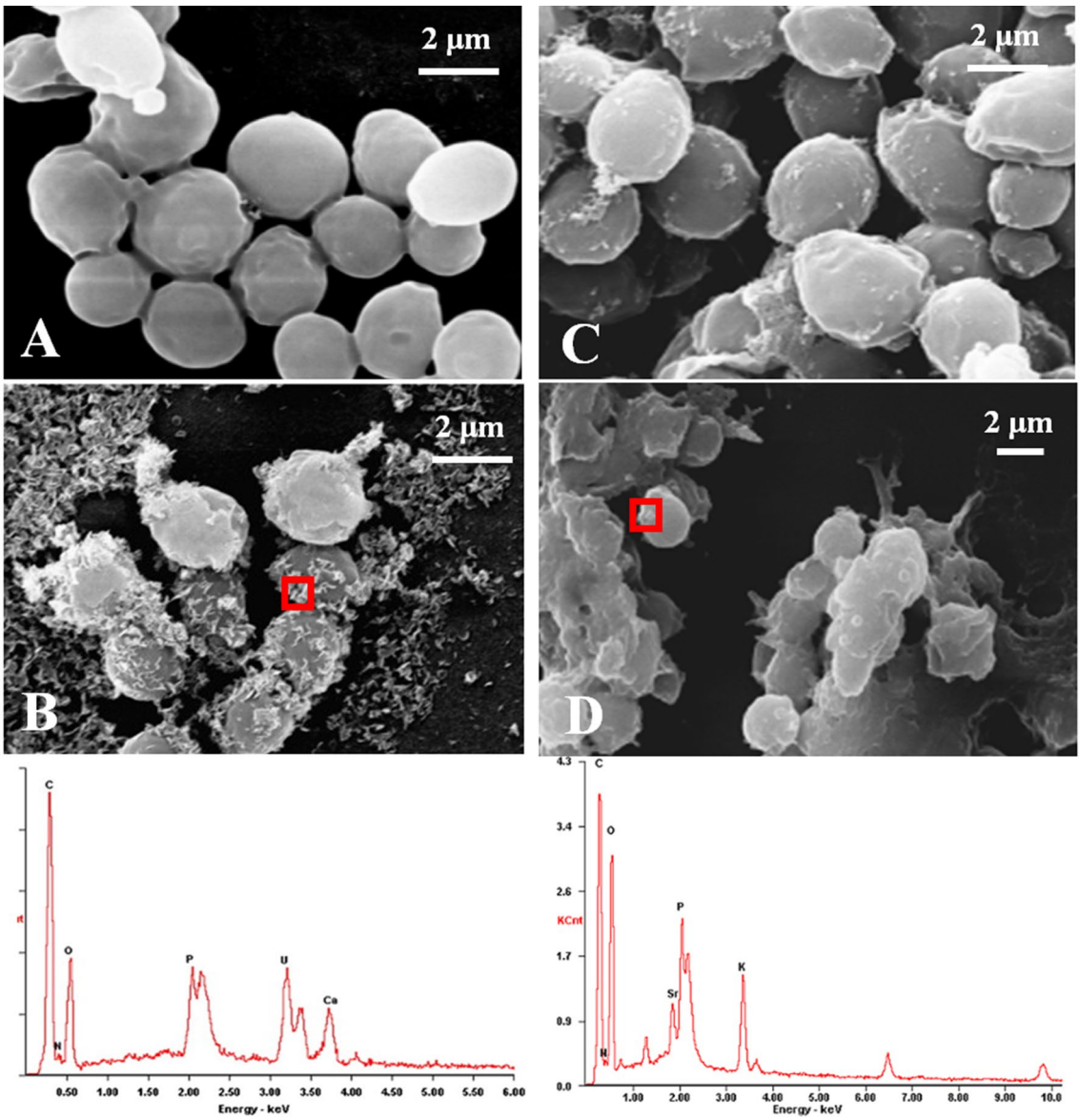

Fig. 2 Morphology of *S. cerevisiae* cells before (**A**, **C**) and after biosorption of uranium (**B**) and strontium (**D**) and EDS analysis

of only a few *S. cerevisiae* cells changed considerably after interacting with uranium. The EDS analysis after biosorption of uranium (Fig. 2) showed that the amount of Ca decreased and that the peak of Na and Mg almost disappeared compared with pristine cells. An obvious new peak of uranium appeared after biosorption, indicating that uranium was absorbed on the cell surface. The uranium amount on *S. cerevisiae* after biosorption was up to 12% (wt%). A substantial increase in P was observed after uranium biosorption. The arise of uranium, the decreased Ca and increased P, with Ca:U:P at 1.2:1.0:1.9 (At%), suggested that the uranium precipitate was perhaps in the form of $Ca[(UO_2)(PO_4)]\cdot 6H_2O$. The ability to precipitate or form minerals may play an important role in microbial antagonism to uranium stress. Extracellular and cellular secretions can interact with uranium to form precipitates or crystals outside the cell, thus reducing the acute lethal effect of high concentrations of uranium [26].

As shown in Fig. 2c, d, there were some granular precipitate particles attached to the cell wall, which might be formed by Sr^{2+} and the surface organic groups of the cells or the medium component. In addition, some cells were broken and deformed. Bacteria spillage of *S. cerevisiae* could also adsorb Sr^{2+} [27]. The EDS analysis of *S. cerevisiae* after biosorption of Sr^{2+} (Fig. 2) showed that the amount of Sr^{2+} increased from 0.3 to 2.5% (wt%) compared with pristine cells. An obvious peak of Sr^{2+} appeared after biosorption, indicating that Sr^{2+} was absorbed on the cell surface. Sr^{2+} absorbed on *B. subtilis* was reported, as the biosorption of Sr^{2+} can interact with two inner-sphere surface complexes, $SOSr^{+}$ and $SOSr(OH)^{2-}$, simulated by diffuse layer modeling [28].

Interaction of uranium and strontium with surface active functional groups of *S. cerevisiae*

The FTIR spectra before and after biosorption of uranium and strontium are shown in Fig. 3. The broad band at 3421 cm^{-1} was assigned to the asymmetric stretching of $–NH_2$ in the amine base of the protein and the stretching vibration of –OH [29]. After absorption, the peak of -OH shifted from 3421 to 3401 cm^{-1}, indicating that hydroxyl groups may be involved in uranium biosorption processes. Protein is one of the main components of the cell wall, and the absorption peak at 1652 cm^{-1} is the C=O bond stretching vibration of the amide I band on the protein [30]. The absorption peaks at 1543 cm^{-1} and 1244 cm^{-1} are the amide II band and the amide III band [31], respectively, and are caused by the N–H bond bending vibration and C–N bond stretching vibration of the secondary amide. After absorption, the peaks of the amide I band and II bands of the protein did not change greatly, and the absorption peak of the amide III band was passivated, indicating that uranyl ions had an obvious coordination effect with this group. 1400 cm^{-1} is assigned to the carboxyl group characteristic absorption peak of the amino acid residues of the peptide side chain [32]. After absorption, the absorption peak shifted 11 cm^{-1} to a high wavenumber, indicating the coordination of the carboxylic anion with uranyl. The peak at 1075 cm^{-1} is the polysaccharide skeleton vibration absorption band of the cell [33], including the stretching vibration of C–OH of saccharide or the P–O–C stretching vibration, which indicated that the carbohydrate on the cell wall was also involved in the biosorption process of uranium. After biosorption of uranium, a new peak appeared at 913 cm^{-1}, which was a vibration of UO_2^{2+} [34] and was direct evidence for uranium absorbed on the *S. cerevisiae* surface.

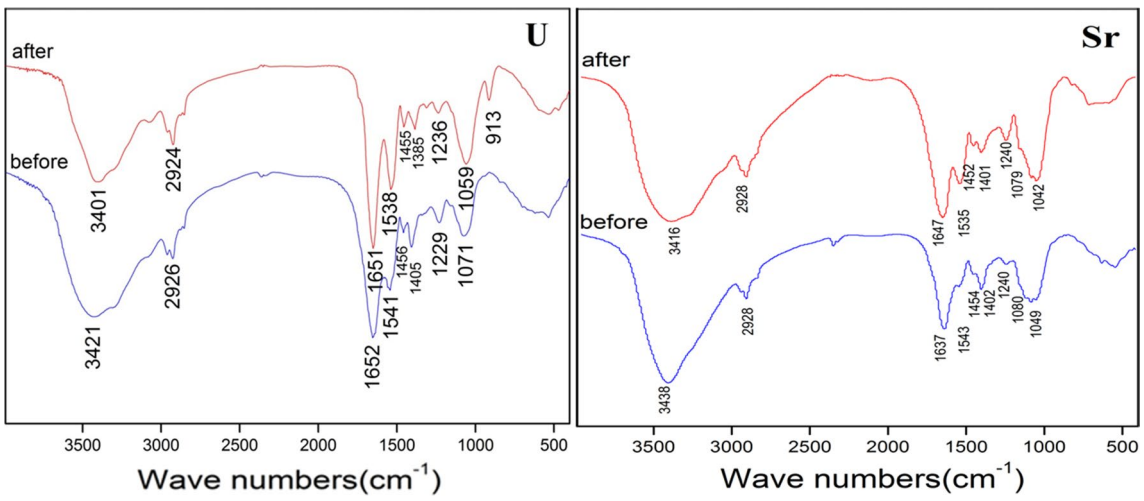

Fig. 3 FTIR spectra of *S. cerevisiae* cells before and after biosorption of uranium (left) and strontium (right)

The FTIR results revealed that the *S. cerevisiae* cell wall was the major biosorption site and that –O–H, –C=O and $–PO_2$ contributed to the major bonding groups. In general, most secondary uranium minerals were composed of uranyl ions. These uranium minerals could present a characteristic peak at 800–1100 cm^{-1}. The EDS results of Ca:U:P were 1.2:1.0:1.9 (at%) in this study. Therefore, the precipitate may be autunite ($Ca[(UO_2)(PO_4)]·6H_2O$) (Fig. 2

The FTIR spectra before and after biosorption of strontium are shown in Fig. 2 (right). The polysaccharide skeleton vibration absorption band (stretching vibration of C–OH of the carbohydrate) of *S. cerevisiae* at 1049 cm^{-1} [33] was increased and shifted to 1042 $cm^{-1,}$ indicating that C–OH groups were involved in the process of Sr^{2+} biosorption. The asymmetric and symmetric bending vibration peaks [δ_{as} (CH_3)] and [δ_s (CH_3)] of the methyl groups in the protein at 1454 cm^{-1} and 1402 cm^{-1} [35] did not change greatly before and after biosorption. The C=O stretching vibrations in the amide I band of the protein amide I band, N–H bending vibrations, N–H bending vibrations and C–N stretching vibrations of amide II are at 1637 cm^{-1} and 1543 cm^{-1} [36], respectively. After biosorption, the amide I and II bands are shifted to high wavenumbers. Similar to uranium, the peak of –OH shifted from 3438 to 3416 cm^{-1}, indicating that hydroxyl groups may be involved in strontium biosorption processes. The FTIR spectra of *S. cerevisiae* cells before and after biosorption of strontium revealed that hydroxyl groups, amino groups and carboxyl groups contributed to the major bonding groups.

Tolerance mechanism of *S. cerevisiae* to uranium and strontium

In response to environmental stress, microorganisms adapt to drastic changes while exerting cellular functions by controlling gene expression, metabolic pathways, enzyme activities, and protein–protein interactions [37]. *S. cerevisiae* transformed the radionuclide occurrence state, but at the same time, the radionuclide could also have some impact on *S. cerevisiae*. The antioxidant enzyme system of *S. cerevisiae* under different concentrations of uranium and strontium stress and reaction times are given in Fig. 4. Strontium had a more toxic effect on cells than uranium. This was because uranyl ions could combine with many complexing ligands to reduce the damage to cells.

Strontium ions caused a rapid increase in malonaldehyde (MDA), an increase in superoxide dismutase (SOD) activity and a decrease in catalase (CAT) enzyme activity in cells at the same concentration, indicating that strontium ions promoted the production of a large number of superoxide

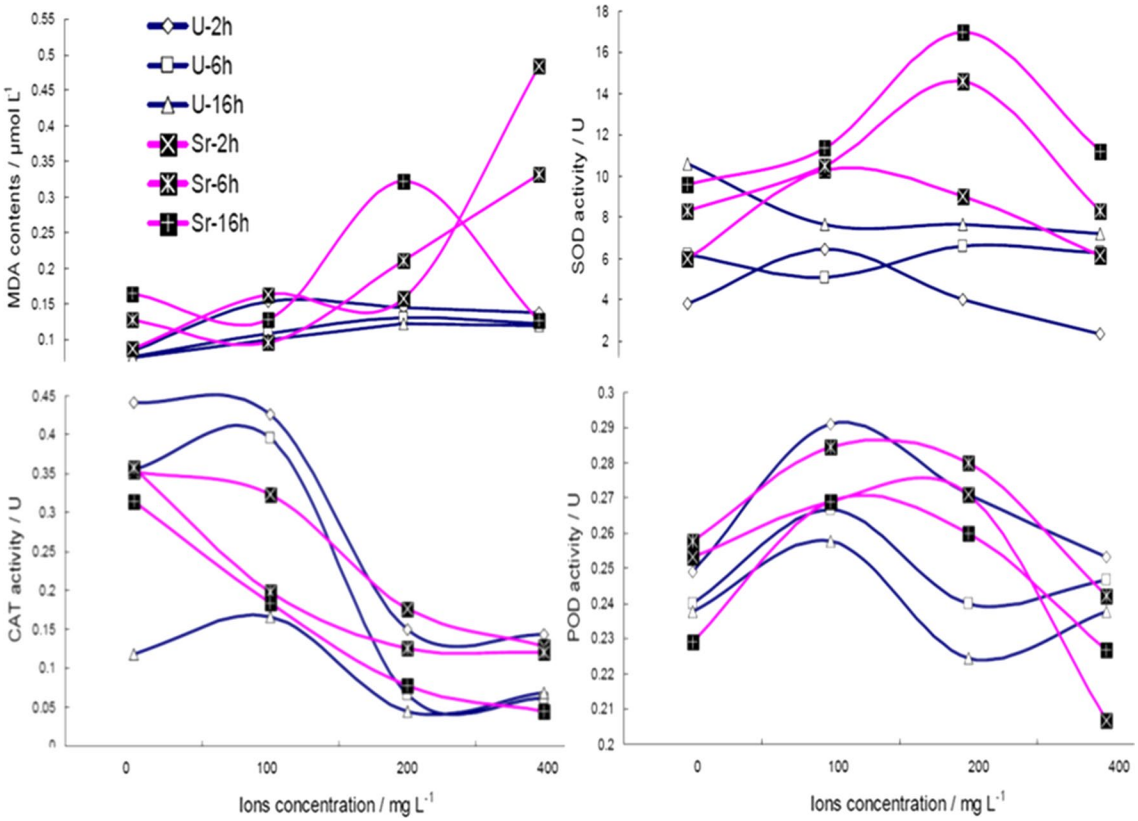

Fig. 4 Antioxidant enzyme system of *S. cerevisiae* under different concentrations of uranium and strontium stress and reaction time

negative anions and hydrogen peroxide in cells and caused lipid peroxidation in the cells [38]. Surprisingly, uranyl ions mainly caused a decrease in CAT activity in cells, which did not generate significant changes in MDA and SOD levels. This means that the increase in hydrogen peroxide resulted in a drop in CAT, but it was not enough to induce lipid peroxidation in cells [39].

At low concentrations, for a short period of time, the antioxidant enzyme system was rapidly activated by *S. cerevisiae* to remove the damage caused by uranium and strontium oxide stress, which contributed to the fluctuation of enzyme activity [40]. With increasing time, the enzyme activity could be expressed steadily, indicating that *S. cerevisiae* had adapted to the stress of low concentrations of uranium and strontium.

At high concentrations, strontium could rapidly cause lipid peroxidation in cells. Therefore, the intracellular oxidation clearance mechanism could be activated over time and alleviate lipid peroxidation in cells. In addition, the extracellular membrane and culture medium could form precipitates with strontium and uranium to reduce the acute lethal effect of high concentrations of uranium and strontium, but high concentrations of uranium and strontium still inhibited the activity of antioxidant enzymes, caused irreversible oxidative damage to membrane lipids, and even led to cell death.

Occurrence state of uranium and strontium after the ashing process

For recycling uranium and strontium, after biosorption enrichment by *S. cerevisiae*, centrifugal separation and the ashing process proceeded. The XRD spectra of *S. cerevisiae* after interacting with uranium (100 mg/L, 24 h) before and after ashing are given in Fig. 5 (left). Three sharp diffraction peaks were observed at diffraction angles of 18.02, 25.62 and 27.41. The results indicated that new crystals were formed after biosorption of uranium by *S. cerevisiae*. After burning for 4 h at 800 °C, the bacteria that precipitated appeared to have a large weight and volume reduction ratio, which suggested that the decomposition of organic matter and some unstable materials in the sediment disappeared gradually. After the ashing process, many new sharp diffraction peaks appeared, and the crystallization was excellent. It was suggested that the main phase after the ashing process was UP_2O_7 (PDF card number 00-003-1196).

The XRD spectra of ash with different initial concentrations of strontium (Fig. 5, right) showed that strontium mainly existed as $SrSO_4$ in ash after biosorption, whereas only a small amount of $SrCO_3$ was found when the concentration of strontium was higher than 200 mg/L. The XRD results also showed that there was little $Sr_3(PO_4)_2$ in the ash when the concentration of strontium was 100 mg/L.

Implications for radionuclide and microorganism

Our experiments described and compared the transformation of two radionuclide occurrence states in microbial recycling and the antioxidant enzyme system of microorganisms under different radionuclide stresses (Fig. 6). Free radionuclide ions will complex with the active groups on the cell surface first and then be adsorbed on the cell surface. After the biosorption process, the adsorbed radionuclide could form special precipitates or even minerals on the envelope. For volume reduction and recycling radionuclides, the ashing process was applied in general, which could yield a volume reduction ratio of more than 1000 times or an approximately 40 times the weight reduction ratio as well as more than 500 enrichment times for radionuclides in ash [8]. The final state of radionuclide after ashing was diversiform on the basis of the kind of radionuclide and experimental conditions, but the final products were stable and reusable. For radionuclides, biosorption-bonding-precipitation or biomineralization processes may be a way to recycle radionuclides, but for microorganisms, they may be a cell detoxification mechanism. These results will help to understand the evolution of

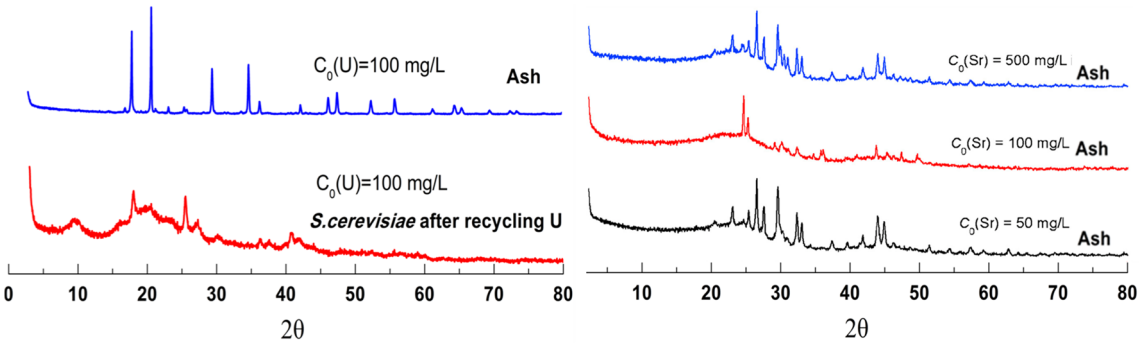

Fig. 5 XRD of *S. cerevisiae* after interacting with uranium (100 mg/L, 24 h) before and after ashing (left) and ashing with different initial concentrations of strontium (right)

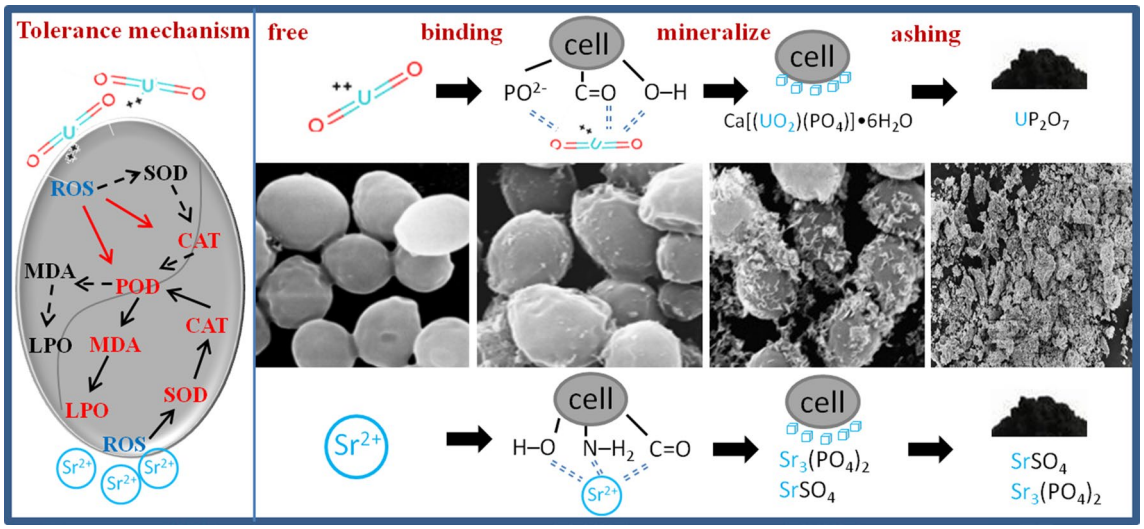

Fig. 6 Transformation of the occurrence state in uranium and strontium recycling by *Saccharomyces cerevisiae* and tolerance mechanism

environmental minerals, such as bioinduced precipitation of autunite and celestite.

Conclusions

The transformation of two radionuclide occurrence states in bio-recycling and the antioxidant enzyme system of microorganisms under uranium and strontium stresses were described and compared. Our major findings are that:

(1) Free uranyl ions will mainly complex with –O–H, –C=O and $–PO_2$ on the cell surface and then become adsorbed. The adsorbed precipitate can be transformed into autunite on the cell surface. The final state of uranium is mainly in the form of UP_2O_7 after ashing.
(2) Free Sr(II) ions will mainly complex with –O–H, $–NH_2$ and –C=O on the cell surface and then become adsorbed. The adsorbed precipitate and the final state of Sr(II) are mainly in the form of $SrSO_4$ after ashing.
(3) Strontium has a more toxic effect on cells than uranium because uranyl ions can combine with many complexing ligands to reduce damage to cells.
(4) The biosorption and ashing environment have implications for the bioinduced precipitation of autunite and celestite.

Acknowledgements This study was supported by the National Natural Science Foundation of China (42007281, 51974261), the Key Project of National Natural Science Foundation of China (41831285), and the National Key Research and Development Program (2018YFC1903304).

Declarations

Conflict of interest The authors declare that they have no conflict of interest.

References

1. Agency ONE (2007) *Nuclear Development Risks and Benefits of Nuclear Energy: Complete Edition - ISBN 9264035516.* Sourceoecd Nuclear Energy, volume 2007: p. i-88(89)
2. Kochkin B et al (2021) Problems and perspectives of borehole disposal of radioactive waste. Prog Nucl Energy 139:103867
3. Ferenbaugh JK et al (2002) Radionuclides in soil and water near a low-level disposal site and potential ecological and human health impacts. Environ Monitor Assess 74:243
4. Banala UK, Das NPI, Toleti SR (2021) Microbial interactions with uranium: Towards an effective bioremediation approach. 101254Environ Technol Innov 21:101254
5. Liu M et al (2010) Biosorption of uranium by *Saccharomyces cerevisiae* and surface interactions under culture conditions. Bioresour Technol 101(22):8573–8580
6. Hu W et al (2017) Synergistic interface behavior of strontium adsorption using mixed microorganisms. Environ Sci Pollut Res Int 25:22368
7. Zhang J et al (2020) Uranium biosorption mechanism model of protonated *Saccharomyces cerevisiae*. J Hazard Mater 385:121588
8. Liu M et al (2016) Programmed gradient descent biosorption of strontium ions by *Saccaromyces cerevisiae* and ashing analysis: a decrement solution for nuclide and heavy metal disposal. J Hazard Mater 314:295–303
9. Chen L et al (2021) Uranium (U) source, speciation, uptake, toxicity and bioremediation strategies in soil-plant system: a review. J Hazard Mater 413:125319
10. Farhan SN, Khadom AA (2015) Biosorption of heavy metals from aqueous solutions by *Saccharomyces cerevisiae*. Int J Ind Chem 6(2):119–130

11. Altimari P, Caprio FD, Pagnanelli F (2017) *Biosorption of Copper by Saccharomyces cerevisiae: From Biomass Characterization to Process Development.*
12. Fadel M et al (2017) Biosorption of manganese from groundwater by biomass of *Saccharomyces cerevisiae*. Hbrc J 13(1):106–113
13. Qiu L et al (2017) Biosorption of the strontium ion by irradiated *Saccharomyces cerevisiae* under culture conditions. J Environ Radioact 172:52–62
14. Zheng XY et al (2017) Biosorption and biomineralization of uranium(VI) by *Saccharomyces cerevisiae*-crystal formation of chernikovite. Chemosphere 175:161–169
15. Liu M et al (2014) Biosorption of strontium from simulated nuclear wastewater by *Scenedesmus spinosus* under culture conditions: adsorption and bioaccumulation processes and models. Int J Environ Res Public Health 11(6):6099–6118
16. Shen Y et al (2018) The biomineralization process of uranium(VI) by *Saccharomyces cerevisiae*—transformation from amorphous U(VI) to crystalline chernikovite. Appl Microbiol Biotechnol 102:4217
17. Hu W et al (2017) Synergistic interface behavior of strontium adsorption using mixed microorganisms. Environmental Science & Pollution Research
18. Pathirana C et al (2022) Biosorption of heavy metals: transferability between batch and column studies. Chemosphere 294:133659
19. Ping Y, Macaskie LE (2010) Removal of the tetravalent actinide thorium from solution by a biocatalytic system. J Chem Technol Biotechnol Biotechnol 64(1):87–95
20. Şimşek S, Yılmaz E, Boztuğ A (2013) Amine-modified maleic anhydride containing terpolymers for the adsorption of uranyl ion in aqueous solutions. J Radioanal Nucl Chem 298(2):923–930
21. Şenol ZM et al (2021) Synthesis and characterization of chitosan–vermiculite composite beads for removal of uranyl ions: isotherm, kinetics and thermodynamics studies. J Radioanal Nucl Chem 327(1):159–173
22. Monnin C (1999) A thermodynamic model for the solubility of barite and celestite in electrolyte solutions and seawater to 200°C and to 1 kbar. Chem Geol 153(1):187–209
23. Monnin C, Galinier C (1988) The solubility of celestite and barite in electrolyte solutions and natural waters at 25°C: A thermodynamic study. Chem Geol 71(4):283–296
24. Merroun ML et al (2005) Complexation of uranium by cells and S-layer sheets of *Bacillus sphaericus* JG-A12. Appl Environ Microbiol 71(9):5532
25. Krueger S et al (1993) Characterization of the Binding of Gallium, Platinum, and Uranium to Pseudomonas fluorescens by Small-Angle X-Ray Scattering and Transmission Electron Microscopy, vol 59. Applied & Environmental Microbiology, pp 4056–4064. 12
26. Wang T et al (2017) Different biosorption mechanisms of Uranium(VI) by live and heat-killed *Saccharomyces cerevisiae* under environmentally relevant conditions. J Environ Radioact 167:92–99
27. Shao XZ (2010) Biosorption of strontium ions by magnetically modified yeast cells. Sep Sci Technol 45(10):1499–1504
28. Guo Y et al (2016) The biosorption of Sr(II) on *Bacillus subtilis*: a combined batch and modeling study. J Mol Liq 220:762–767
29. Wang Q et al (2007) Alginate/polyethylene glycol blend fibers and their properties for drug controlled release. J Biomedical Mater Res Part A 82(1):122–128
30. Gniadecka M et al (2004) Melanoma diagnosis by Raman spectroscopy and neural networks: structure alterations in proteins and lipids in intact cancer tissue. J Invest Dermatology 122(2):443–449
31. Huang CY, Balakrishnan G, Spiro TG (2006) Protein secondary structure from deep-UV resonance Raman spectroscopy. J Raman Spectrosc 37(1–3):277–282
32. Barth A (2000) The infrared absorption of amino acid side chains. Prog Biophys Mol Biol 74(3):141–173
33. Schwanninger M et al (2004) Effects of short-time vibratory ball milling on the shape of FT-IR spectra of wood and cellulose. Vib Spectrosc 36(1):23–40
34. Ramos ML et al (2017) Oxocomplexes of U (vi) with 8-hydroxyquinoline-5-sulfonate in solution: structural studies and photophysical behaviour. Dalton Trans 46:9358–9368
35. Fan X, Xu N-J, Shi J-G (2003) Bromophenols from the Red Alga Rhodomela confervoides. J Nat Prod 66(3):455–458
36. Palaniappan PR, Pramod K (2010) FTIR study of the effect of nTiO2 on the biochemical constituents of gill tissues of Zebrafish (*Danio rerio*). Food Chem Toxicol 48(8):2337–2343
37. Takagi H (2021) Molecular mechanisms and highly-functional development for stress tolerance of the yeast *Saccharomyces cerevisiae*. Biosci Biotechnol Biochem 85:1017–1035
38. Zhang J, Kirkham M (1994) Drought-stress-induced changes in activities of superoxide dismutase, catalase, and peroxidase in wheat species. Plant Cell Physiol 35(5):785–791
39. Demiral T, Türkan I (2005) Comparative lipid peroxidation, antioxidant defense systems and proline content in roots of two rice cultivars differing in salt tolerance. Environ Exp Bot 53(3):247–257
40. Wilmsen PK, Spada DS, Salvador M (2005) Antioxidant activity of the flavonoid hesperidin in chemical and biological systems. J Agric Food Chem 53(12):4757–4761